

Experimental Investigation of a LOX/Methane Liquid-Centered Swirl Coaxial Injector During Ignition, Startup and Subcritical Operation

Alexander Bee^{*}, Michael Börner[†] and Justin S. Hardi[†]

^{*} [†] Institute of Space Propulsion, German Aerospace Center (DLR), 74239 Hardthausen, Germany

^{*}Alexander.Bee@dlr.de

^{*}Corresponding author

Abstract

In the context of the ever-growing interest in liquid oxygen and methane as a propellant combination for liquid rocket engines, swirl coaxial injectors have been found to present an interesting alternative to the shear coaxial injectors classically used in European launcher engines. By not only relying on shear, but also on centrifugal forces as well as propellant impingement, swirl coaxial injectors can offer improved propellant atomization compared to shear injectors. This could lead to improved flame anchoring characteristics for liquid oxygen/methane flames, especially under varying operating conditions like deep-throttling. By retaining geometric and operational similarities, they also allow for simple interchangeability with shear injectors, especially when compared to other injector types. However, publicly available experimental data, especially from hot-fire tests of such elements, is very limited. For this purpose, a single liquid-centered swirl coaxial injector operating with liquid oxygen and gaseous methane is designed and hot-fire tested at the M3.1 testbench at the German Aerospace Center (DLR) Institute of Space Propulsion in Lampoldshausen, Germany. The injector is designed to be representative of elements of main stage combustion chambers previously found in industrial and literature applications. The liquid oxygen is swirled by the use of tangential inlet holes. Compared to the liquid-centered swirl injectors commonly found in literature, the element presented in this study features a special fuel annulus in which, through the use of specifically designed guiding vanes, tangential momentum is also applied on the methane flow. Additive manufacturing is used to create the sophisticated methane annulus geometries. Cold-flow studies as well as hot-fire tests are conducted in an optically accessible subscale combustor with a 60-millimeter diameter. The experiments are accompanied by high-speed Schlieren diagnostics as well as high speed OH^{*}-visualization techniques. The focus of the hot-fire testing is the investigation of the injector's behavior during ignition and the startup transient phase, as well as during short quasi steady-state operation at low, subcritical pressures between 2.5 and 3.2 bar. Ignition is achieved via a pulsed laser ignition system. Important injector characteristics such as spray shape, flame topology, as well as combustion stability are investigated in this study. The performances of different injector geometries (co- and counter swirling methane flow) with regard to these characteristics are compared and evaluated accordingly.

1. Introduction

In recent years, the propellant combination of liquid oxygen (LOX) and methane (CH₄), or the closely-related liquid natural gas (LNG), has positioned itself as one of the most popular choices for current and future liquid rocket engine (LRE) development projects. Besides the well-known American LOX/CH₄ LREs like SpaceX's *Raptor* engine or Blue Origin's *BE-4* engine, LOX/CH₄ has also found its way into the European launcher propulsion sector, with the most popular example being the *Prometheus* engine currently under development by ArianeGroup [8]. For every LRE, the injector of the main combustion chamber (MCC) is one of the most critical subsystems as many important engine characteristics such as combustion efficiency and stability, wall heat loads and other considerations like throttleability depend on its performance. In Europe, with its long lasting heritage in LOX/hydrogen gas-generator and expander cycle engines, the injector element of choice so far has been the shear coaxial injector [6]. However, these injector types have shown potential problems in flame anchoring and combustion stability when operated with LOX/CH₄ [9, 12, 15]. Swirl coaxial injectors might offer an interesting alternative to the classical shear injectors. In swirl coaxial injectors, a tangential momentum is applied to one or both of the propellants. For large cryogenic gas-generator or expander-cycled

LREs following European design, the LOX is injected in its liquid state while the fuel is most commonly injected in its gaseous (or low-density supercritical) state after heat input from the regenerative cooling circuit. As a result of the tangential momentum imposed onto the LOX, a thin swirling sheet forms at the inner wall of the LOX post with a central gaseous core spanning the entire length of the element's post [11]. When exiting the post, no longer confined by walls this sheet expands as a result of the centrifugal forces, in the radial direction in the form of a hollow cone. Such elements are called liquid-centered swirl coaxial injectors (LCSCIs).

Potentially, these LCSCIs could offer increased atomization and combustion efficiency by not only relying on the shear forces generated by the propellants' velocity difference for propellant breakup, like their shear counterparts, but also on the centrifugal forces and the resulting thinning of the liquid sheet in the injector exit spray cone. Additionally, the impingement of the high velocity gas co-flow onto said thin sheet also leads to fast and violent liquid propellant breakup. The following section will give a brief overview on LCSCI design theory and its most important parameters.

2. Swirl Injector Design Theory

Figure 1 shows a schematic of a typical LCSCI element and its different sections. Fundamentally, a LCSCI consists of a liquid (oxidizer in this case) side and a gaseous (fuel) side.

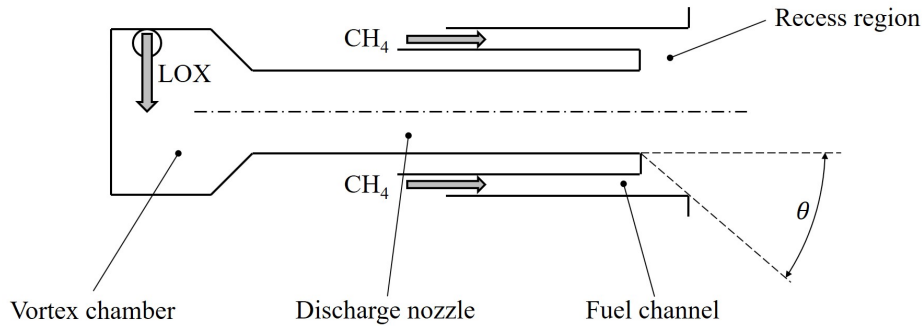


Figure 1: Schematic depiction of a generic liquid-centered swirl coaxial injector.

The liquid side can be divided into a vortex chamber and a discharge nozzle. The liquid oxidizer enters the vortex chamber (with its radius R_V) through the tangential inlets (inlet radius R_{inlet}). The resulting tangential momentum is produced by the inlet velocity V_{inlet} and the swirl arm length. The swirl arm length is calculated as the distance between the vortex chamber's center axis and the central axis of the inlet ports ($R_V - R_{inlet}$). The ratio of the swirl arm length and the discharge nozzle radius R_N can be expressed by the contraction coefficient β as follows:

$$\beta = \frac{R_V - R_{inlet}}{R_N} \quad (1)$$

Depending on the value of β , pressure swirl injectors can be divided into two types:

- $\beta \leq 0$: The injector's vortex chamber diameter is identical or smaller compared to the discharge nozzle diameter. Because of the absence of a convergent section, the injector post can be seen as a long, open-ended vortex chamber. Therefore, these injectors are called open-end injectors.
- $\beta > 0$: The injector has a larger vortex chamber diameter compared to its discharge nozzle. These injectors are called closed-end injectors.

For every tangential inlet pressure swirl injector, open or closed-end type, a characteristic geometric constant K can be defined. K is defined as the ratio between (tangential) inlet velocity and axial fluid velocity for a fully flowed through nozzle multiplied with the contraction coefficient. With a known value for K , the following relation can be found [1]:

$$K = \frac{V_{inlet}}{V_{axial,full}} \beta = \frac{(1 - \phi) \sqrt{2}}{\phi \sqrt{\phi}} \quad (2)$$

with ϕ being the coefficient of passage fullness. The coefficient of passage fullness is defined as the ratio of the cross sectional area of the injector post used by the swirling liquid film and its total cross sectional area. From ϕ , the

tangential-to-axial velocity ratio of the swirling flow (VR), and further, the half spray angle of the free liquid spray cone α can be determined via the following relations:

$$\frac{V_{\tan}}{V_{\text{axial}}} = \tan \alpha = \tan \frac{2(1 - \phi)^2}{2 - \phi - 2(1 - \phi)^2} \quad (3)$$

These relations form the most basic design theory of pressure swirl injectors, however they are only applicable for tangential slot type atomizers. As a more general characteristic parameter, the swirl number can be used. The swirl number SN is defined as the ratio between axial flux of angular momentum and axial flux of axial momentum [4]. For swirlers that generate tangential momentum with the help of guiding vanes in an annular channel, SN can be calculated via:

$$SN = \frac{2}{3} \left(\frac{1 - (R_1/R_O)^3}{1 - (R_1/R_O)^2} \right) \tan \alpha \quad (4)$$

with α being the deflection angle of the vanes. R_1 and R_O are the inner and outer radii of the annular channel. This can also be modified for use in tangential inlet type swirlers. Then, Equation 4 simplifies (due to the absence of a central hub) to $SN = 2/3 \tan \alpha$, with α as the free oxidizer spray cone angle that can be deduced from Equation 3.

Like their shear injector counterparts, LCSCIs can feature a recessed oxidizer post, thus creating a recess region (as shown in Figure 1). The angle between the oxidizer post exit diameter and the fuel channel exit diameter, θ , is known as the recess angle. If θ is larger than the spray angle α , the liquid sheet will not reach the fuel channel inner wall, thus mixing of the two propellants will primarily occur outside of the recess region. This configuration is called an *outer-mixing-flow* LCSCI. Conversely, if $\theta < \alpha$, the liquid sheet can impact the wall creating an *inner-mixing-flow* LCSCI. The edge case, where $\theta = \alpha$ is called a critical recess configuration. To evaluate recess criticality, a normalized recess length \tilde{L}_R can be defined as

$$\tilde{L}_R = \frac{L_R}{L_{R,\text{crit}}} = \frac{L_R}{R_1 - R_N} \tan \alpha \quad (5)$$

with the recess length L_R and the critical recess length $L_{R,\text{crit}}$ (where $\alpha = \theta$). For the critical recess configuration \tilde{L}_R equals to 1. Water testing in literature has shown that the best atomization performance for LCSCIs is achieved, when the recess length is slightly overcritical [17]. Another important design parameter of LCSCI elements is the (axial) momentum flux ratio J_{axial} . It is calculated as the ratio of fuel and oxidizer momentum flux ratios via

$$J_{\text{axial}} = \frac{\rho_{\text{fuel}} V_{\text{axial,fuel}}^2}{\rho_{\text{LOX}} V_{\text{axial,LOX}}^2} \quad (6)$$

where ρ_i and $V_{\text{axial},i}$ are the density and axial injection velocities for the respective propellants i .

3. Experimental Setup

3.1 Injector Element

The injector element hot-fired in this study was designed to be representative, both in size and operational boundary conditions, of injector elements used in MCCs of main-stage rocket engines. The design point and corresponding mass flow rates for the swirl injector element is that of a generic LOX/CH₄ shear coaxial element defined for the by REST (Rocket Engine Stability initiative) as a numerical test case [10, 13, 14]. The LCSCI element in this study was furthermore designed to be of comparable dimensions to the REST shear coaxial element. Parameters specific to swirl injectors were found by applying common design rules and experiences for such elements to target for optimal performance. The injector element's relevant characteristic parameters can be found in Table 2.

Figure 2 shows a schematic cross section of the injector head with the integrated single LCSCI element. Fundamentally, the element consists of the central LOX post (A) and the fuel sleeve (B). With the help of a tightening nut (C), the fuel sleeve is fixed to the faceplate (D), which separates the combustion chamber volume (E) from the fuel manifold, also called fuel dome (F). The LOX dome (G) is at the back end of the injector head, separated from the fuel dome by the inter-propellant plate. From here, LOX enters the post through four tangential entry ports (H), while the CH₄ enters the fuel sleeve through a number of radial entries. Subsequently, CH₄ flows through the annular fuel gap, in which a series of guiding vanes (I) are used to achieve different CH₄ injection configurations. These configurations include:

- Coaxial CH₄ injection (CX): The guiding vanes are straight (see Figure 2, top-right).

EXPERIMENTAL INVESTIGATION OF A LOX/CH₄ SWIRL COAXIAL INJECTOR DURING SUBCRITICAL OPERATION

- Co-swirling CH₄ injection (CO): The guiding vanes are bent in a clockwise manner, imposing an angular momentum onto the CH₄ flow, resulting in a co-swirling motion compared to the LOX injector (see Figure 2, middle-right).
- Counter-swirling CH₄ injection (CT): The guiding vanes are bent in a counter-clockwise manner, imposing an angular momentum onto the CH₄ flow, resulting in a counter-swirling motion compared to the LOX injector (see Figure 2, bottom-right).

Additionally, the guiding vanes also act as a support structure to keep the LOX post centered inside the fuel sleeve, guaranteeing uniform fuel gap width around the circumference of the injector element. The deflection angles of the guiding vanes are 0°, +20°, and -20° for the coaxial, co-, and counter-swirling configuration, respectively. The chosen deflection angle ensures that the angular momentum of the methane is significantly lower compared to the oxidizer side. The swirl numbers and expected velocity ratios as defined in Equation 3 and 4 for the configurations are listed in Table 1. The required channel radius ratio R_1/R_0 for calculating the CH₄ swirl number of the tested injector element is 0.9.

Table 1: Overview of tested LCSCI element configurations with their respective swirl numbers and tangential-to-axial velocity ratios.

ID	Configuration	SN _{LOX}	SN _{CH₄}	VR _{LOX}	VR _{CH₄}
CX	Coaxial CH ₄ injection	0.417	0	0.623	0
CO	Co-swirling CH ₄ injection	0.417	0.024	0.623	0.364
CT	Counter-swirling CH ₄ injection	0.417	0.024	0.623	0.364

Generally, LCSCI elements do not feature an additional tangential momentum on the fuel side. However, studies by Greene et al. [7] have shown that by imposing a co-swirling motion onto the gaseous flow, atomization and therefore combustion efficiency can be potentially increased. While Greene et al. also used tangential inlets to generate the fuel swirl, another study conducted by Ahn et al. [2] featured an additively manufactured swirler helix just upstream of the fuel channel in a separate fuel vortex chamber. Both methods are not seen as ideal solutions for imposing a tangential momentum onto the fuel, because low-density gaseous media aren't able to carry tangential momentum as well or as far compared to incompressible liquids. Therefore, in the design presented in this study, the guiding vanes are placed directly in the fuel channel as close to the injector exit as possible, just upstream of the recess zone. The leading and trailing edges of the guiding vanes are also tapered to minimize flow disturbance.

The injector post's recess length was set so that the normalized recess \bar{L}_R is slightly greater than 1, what promises maximal theoretical atomization efficiency. The axial momentum flux ratio of the injector J_{axial} (see Equation 6) was also chosen to be quite high for a typical LCSCI element, which should further help atomization performance and combustion stability [16]. Higher- J injectors should also help in reducing expected face and wall heat loads, as the combined oxidizer-fuel spray angle decreases with increasing J_{axial} [3].

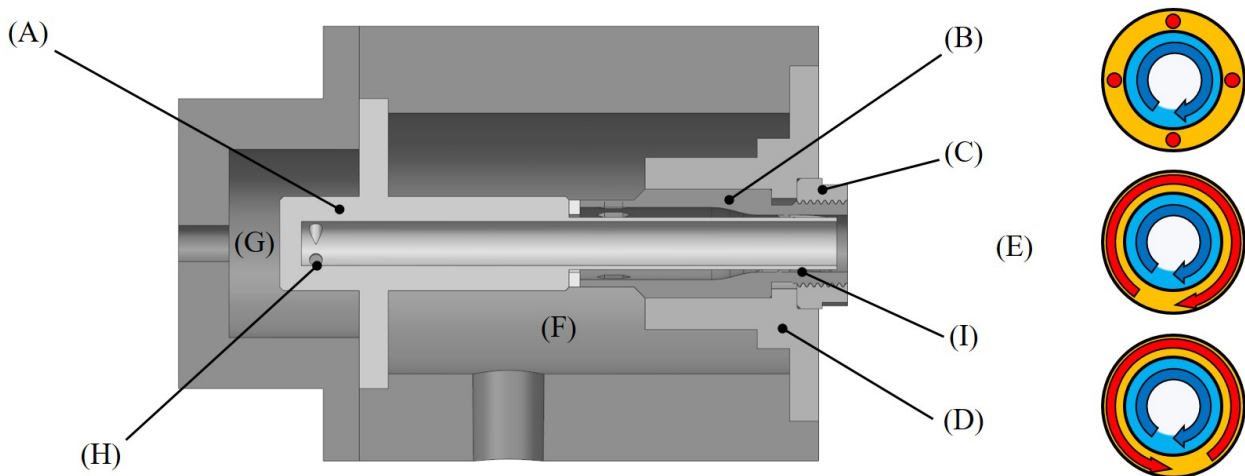


Figure 2: Schematic overview tested LCSCI (left) element and methane injection configurations (right).

Table 2: Characteristic parameters of tested LCSCI element at design point ($P_{CC} = 100$ bar).

Parameter	Symbol	Value
Nominal LOX mass flow rate	\dot{m}_{LOX}	0.461 kg/s
Nominal Fuel mass flow rate	\dot{m}_{Fuel}	0.137 kg/s
Full oxidizer spray cone angle	2α	62° ¹
Characteristic geometric constant	K	2.02
LOX post normalized length	L/D	20.0 ²
Normalized recess length	\tilde{L}_R	1.03
Axial momentum flux ratio	J_{axial}	1.38
Design pressure drop (LOX)	ΔP_{LOX}	22 bar \pm 10%
Design pressure drop (Fuel)	ΔP_{Fuel}	15 bar \pm 10%

This injector element as presented in Table 2 is designed for a future full-scale hot-fire campaign under representative conditions. For the sub-scale ignition test campaign shown in this study, the elements length is shortened by 50% to a L/D -ratio of 10.0 (as measured from the LOX post tip to the tangential inlet hole plane). While the other injector characteristics remain relatively unchanged, the elements spray cone angle is slightly larger compared to the design point, due to reduced viscous losses as a result of the shorter post. However, such a small deviation in spray angle is considered negligible for overall injector performance and behavior.

3.2 Setup at Test Bench

Figure 3 shows a schematic overview of the experimental setup at the M3.1 test bench [5]. The optically accessible micro-combustor with the integrated LCSCI element is directly attached to the test bench's thrust frame. The combustion volume of the combustor is of quasi cylindrical shape with an diameter of 60 mm. The cylindrical shape is broken up by the two plane optical access windows on the sides. The distance between the windows is 54 mm. The optically accessible area is 37 mm high and features a width of 113 mm.

The test bench supplies gaseous methane at close-to ambient temperatures. LOX is produced at the test bench from gaseous oxygen stored in high pressure bottles with the help of a liquid nitrogen bath. The LOX run tank is placed close to the combustor to minimize heat input during the test runs. This allows for low, representative LOX temperatures. The LOX tank, with a volume of 2 L is pressurized with gaseous helium. Helium and methane feed pressures are set with two pressure regulators. CH₄ is supplied directly from high pressure gas storage bundles. The oxidizer and fuel run valves are positioned closely to the injector head and are opened via the release of an electromagnet. With this method, fast and highly reproducible opening times are ensured. The oxidizer feed system and dome is purged with gaseous helium, while the fuel feed system and dome is purged with gaseous nitrogen. The nozzle of the combustor is attached to a tank with a volume of 1500 L, which can be either evacuated or pressurized with nitrogen to simulate different environmental conditions before and during ignition. Ignition of the injector element is achieved with a laser ignition system consisting of a NdYAG-Laser which sends a series of short-duration pulses through an ignition port into the combustion volume. With the help of a lens, the laser pulses are focused onto a predefined spot in the shear layer between the LOX film and the gaseous CH₄ co-flow, where an ignition plasma is subsequently generated by the pulse energy. In total, five laser pulses separated by 20 ms each are fired into the shear layer.

Propellant mass flow rates are measured using two coriolis flow meters. Chamber and dome pressures are recorded using Kister 4043A piezoresistive absolute pressure transducers, while temperatures are measured with type K thermocouples. Sampling rate is 10 kHz for the pressure sensors and 1 kHz for the thermocouples, respectively.

The experiment is supported by an optical diagnostics setup, consisting of two high-speed cameras and a high-power 450 W xenon arc lamp acting as a back-light source. Light emitted from the lamp is redirected through both windows of the combustor with the help of a parabolic mirror. This creates nearly parallel beams. On the other side of the combustion chamber a beam splitter redirects the ultraviolet wavelengths to the image intensified camera (*Photron FASTCAM-APX I2*) which is used for high-speed OH*-visualization. Visible light is, over another mirror, passed over a Schlieren knife edge to the second camera (*Photron SA-X*). The used camera settings are listed in Table 3. Spatial resolution of the two diagnostics are 0.36 mm per pixel (OH*) and 0.124 mm per pixel (Schlieren), respectively.

¹64° for M3.1 tests

²10.0 for M3.1 tests

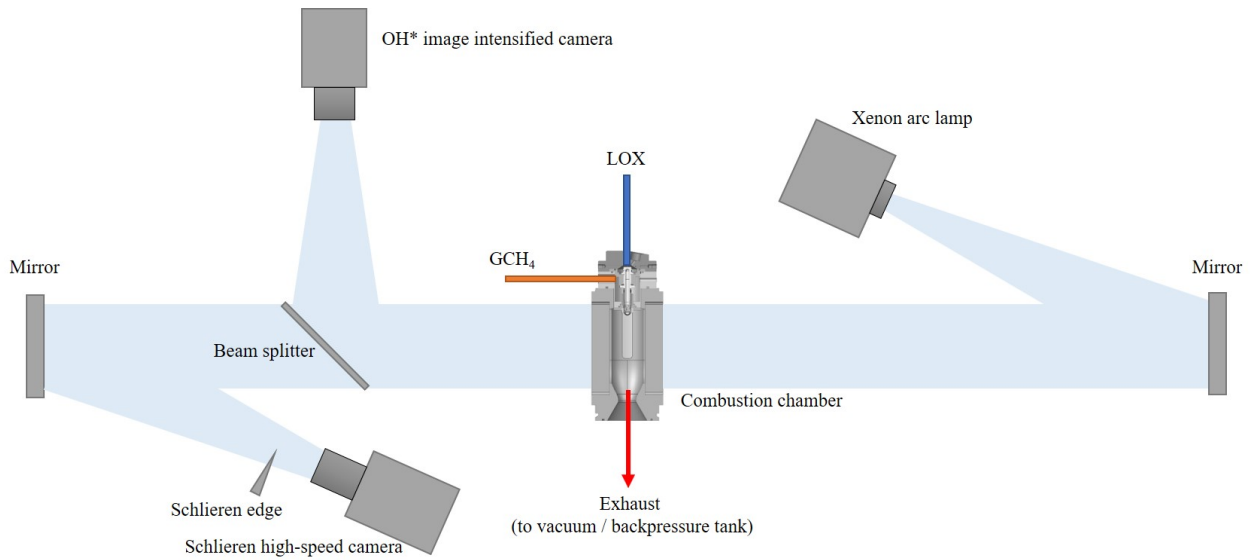
EXPERIMENTAL INVESTIGATION OF A LOX/CH₄ SWIRL COAXIAL INJECTOR DURING SUBCRITICAL OPERATION

Figure 3: Schematic overview of experimental setup at the M3.1 testbench.



Figure 4: Photo of injector element integrated into the M3.1 micro-combustor.

Table 3: High-speed camera and image intensifier settings for all test runs

	APX I2	SA-X
Frame rate	10000 fps	19200 fps
Resolution	512 × 128 px	1024 × 376 px
Shutter	1/frame s	1/400000 s
Gain	4.0	-
Width	10 μs	-

3.3 Operational Boundary Conditions and Testing Goals.

The test duration at the M3.1 testbench is limited due to the absence of a active cooling system. The combustion chamber and nozzle are capacitively cooled. The test runs consist of about 750 ms of hot-fire duration each. Of these 750 ms, the ignition and startup phase is of around 100 ms duration, as is the shutdown phase. Quasi "steady-state" conditions are reached for roughly 500 ms. However, during this timeframe, no thermal equilibrium of the test hardware can be reached. Mass flow rates and propellant injection temperatures are listed in Table 4. The mass ratio of oxidizer-to-fuel (ROF) is set to be 3.4 for the quasi steady-state phase of all test runs. The tests are conducted against nitrogen at 1 bar into a large backpressure tank. To avoid overly high pressure peaks in the case of a delayed ignition, a larger than nominal nozzle throat diameter is used. Target chamber pressure after ignition is set to be at a minimum of 2.5 bar

to ensure choked flow conditions in the nozzle throat. Two different load points (LP1 and LP2) are investigated, LP1 with 2.5 bar of steady-state chamber pressure and LP2 with an increased 3.2 bar of steady-state chamber pressure (see Table 4). The goals of the subscale hot-fire campaign are summarized as follows:

- Goal 1: Investigation of the ignition characteristics of a representative LCSCI element when using a laser ignition system
- Goal 2: Characterization of combustion behavior of the designed element during low subcritical chamber pressures
- Goal 3: Comparison of the three fuel channel geometries and identification of the most suitable configuration for a future fullscale representative hot-fire campaign

Table 4: Target load point after ignition and chamber information.

Parameter	Symbol	LP1	LP2
Target chamber pressure	P_{CC}	2.5 bar	3.2 bar
Maximum LOX mass flow rate	\dot{m}_{LOX}	61.0 g/s	71.2 g/s
LOX injection temperature	T_{LOX}	94...98 K	94...98 K
Maximum fuel mass flow rate	\dot{m}_{Fuel}	17.9 g/s	20.1 g/s
Fuel injection temperature	T_{Fuel}	240...260 K	240...260 K
Chamber combustion volume diameter	D_{CC}	60.0 mm	
Chamber nozzle throat diameter	D_{Nozzle}	26.6 mm	

4. Experimental Results

In this section the results of the subscale hot-fire campaign at the M3.1 testbench are presented. First, the element's performances during the quasi steady-state operation are evaluated with both the help of pressure data and the optical data. Later, the transient ignition behavior of the LCSCI element is evaluated and presented.

4.1 Subcritical Injector Element Operation

4.1.1 Injector Element Performance

Figure 5 shows the combustion chamber pressure and the respective propellant pressure drops for a typical test run. Ignition occurs shortly after the onset of CH₄ injection. Ignition peaks are low (< 8 bar) for all test runs. The test runs for LP1 show a low-frequency (LF) instability with pressure oscillation frequency in the range of around 133 Hz. Such LF instabilities are to be expected when hot-firing an injector element so far below its nominal design point, as both mass flow rate as well as oxidizer pressure drop are not sufficient for stable operation. The LF instability is significantly reduced for LP2, further suggesting that insufficient element mass flow rates contributed to their emergence. All three injector configurations perform quite similarly, with no recognizable influence of CH₄ injection geometry on the LF instability. The only noticeable difference is in fuel side pressure drop, where the coaxial injection element (Figure 5(a+b)) features a slightly lower ΔP compared to the other configurations. This is also expected as, for this element no additional pressure drop is generated by flow deflection. However, pressure drop difference was still within the acceptable deviation boundaries of $\pm 10\%$ (see Table 2) compared to the other configurations.

4.1.2 Optical Diagnostics

Time-averaged images captured by the Schlieren imaging system during both the cold-flow tests and the subsequent hot-runs are shown in Figure 6. The depicted mean images are exclusively from test runs at LP2, to ensure minimal influence of LF pressure oscillations on the flame images. On the left side of Figure 6, the cold-flow images of LOX/CH₄ co-injection are depicted (1a-c), while on the right side the corresponding steady-state hot-fires are shown (2a-c). The images are time-averaged over the quasi steady-state phase of the test runs, between 100 and 600 ms after ignition. Only slight differences can be seen for the cold-gas images: The coaxial element (1a) exhibits, after an initial region of low expansion angle, a rapid broadening of the spray cone. A more gradual broadening with a slimmer maximum radial expansion can be identified for the co-swirling configuration (1b), while the counter-swirling injector (1c) features both the lowest expansion angle as well as the smallest maximum radial expansion further downstream.

EXPERIMENTAL INVESTIGATION OF A LOX/CH₄ SWIRL COAXIAL INJECTOR DURING SUBCRITICAL OPERATION

This is in line with findings by Ahn et al. [2], who, in tests with water and gaseous nitrogen, also reported a smaller combined spray angle for their counter-swirling LCSCI configuration compared to the other elements.

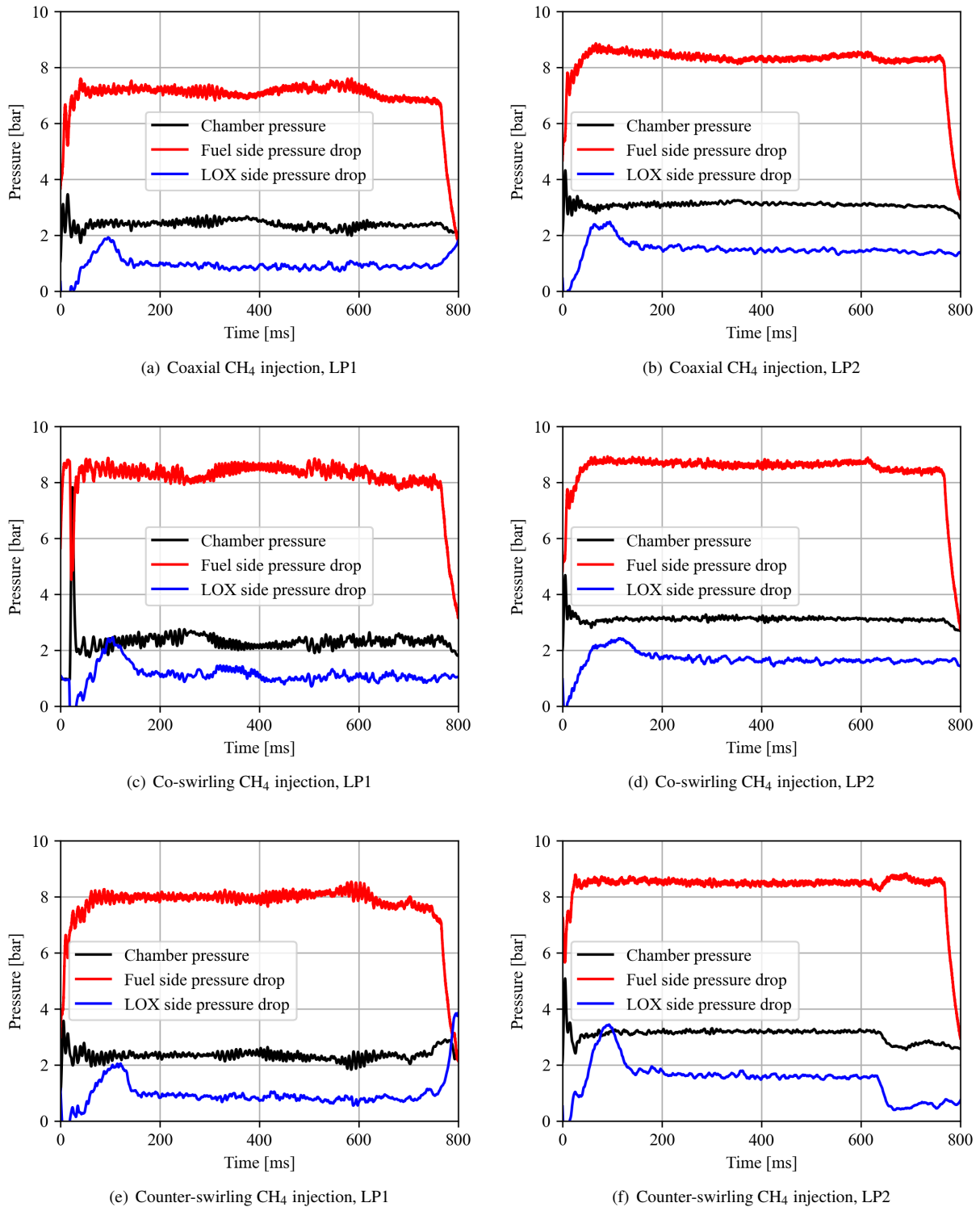


Figure 5: Chamber pressures and propellant pressure drops over injector element over time for the three injector configurations and both load points.

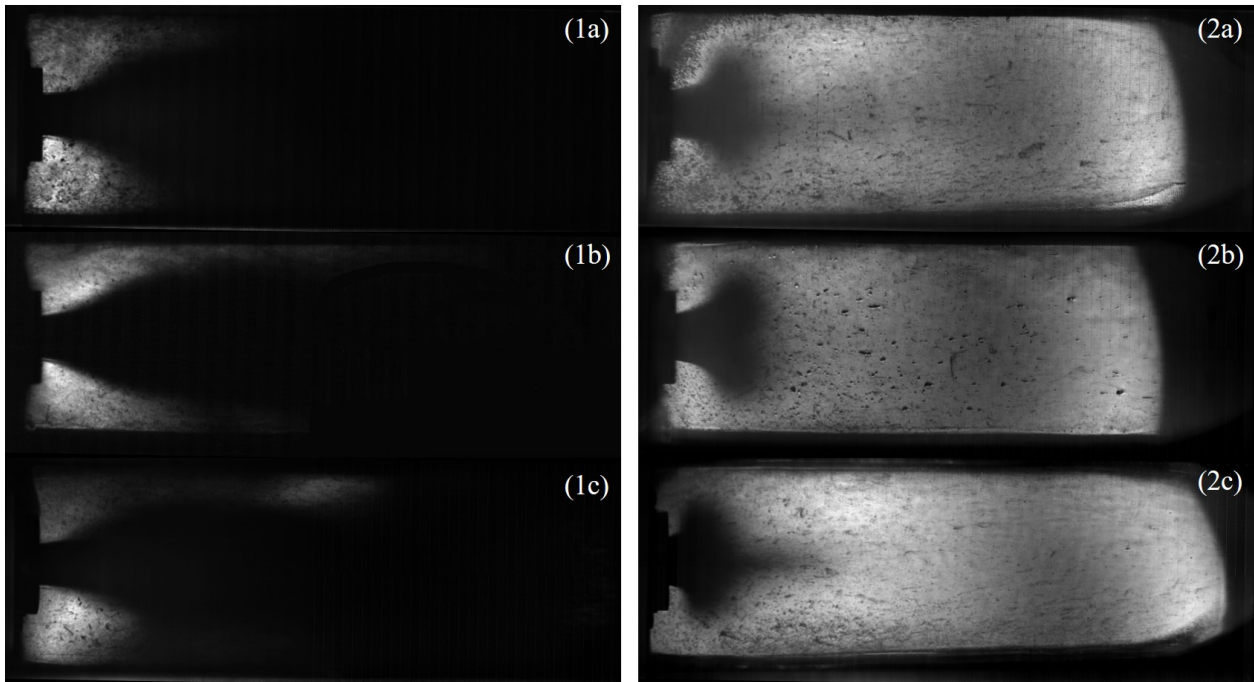


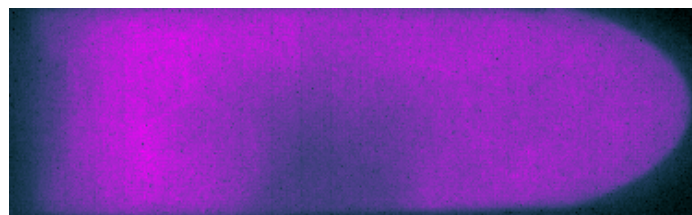
Figure 6: Mean cold-flow (1) and hot-run (2) images of the three tested injector configurations: (a) coaxial CH₄, (b) co-swirling CH₄ and (c) counter-swirling CH₄.



(a) Coaxial CH₄ injection



(b) Co-swirling CH₄ injection



(c) Counter-swirling CH₄ injection

Figure 7: Mean images of high-speed OH* visualization for the three tested injector configurations

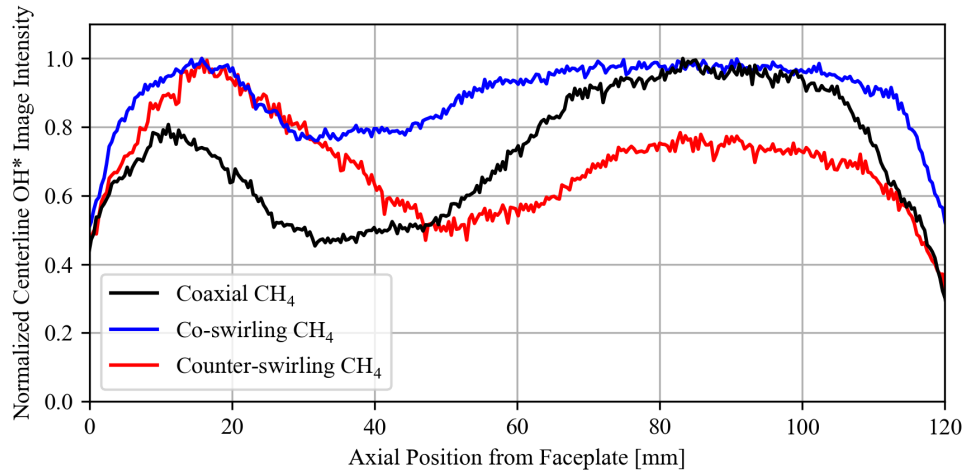


Figure 8: Normalized centerline intensities of mean OH* images for the three injector configurations over axial distance from injector faceplate.

Figure 7 shows the time-averaged images during the quasi steady-state operation. Due to high OH* emissions in the recircularization zone, the flame shape itself is not seen clearly. These recircularization zones are probably a result of the large combustion chamber diameter compared to the injector element as well as the high momentum flux ratio of the injector when operated at such low chamber pressures. Unfortunately, the image intensified camera has a region of bad sensor/intensifier performance, clearly visible in Figure 7 as a darker area in the lower middle of the images. This in addition to potential changes of the image position on the camera chip, prohibits a quantitative comparison between the three configurations. However, a qualitative analysis is conducted by normalizing the OH* intensities along the combustion chamber's center axes for the three cases. The normalized intensities of the mean OH*-images in Figure 7 along the combustion chamber centerline are shown in Figure 8. Intensity is plotted over the (axial) distance from the faceplate. It becomes clear that there are significant differences between the three injector configurations when comparing the axial position of their respective OH*-intensity maximum. The coaxial CH₄ injection configuration features lower intensity close towards the faceplate, with the downstream region clearly dominating. For the co-swirling configuration, intensities close to the injector and downstream are of similar magnitude, while the counter-swirling injector exhibits its maximum near the faceplate with reduced intensity further downstream. This is in line with the findings from Figure 6, where the counter-swirling configuration features a shorter remaining LOX core, possibly indicating faster mixing and breakup with subsequent higher reactivity close to the injection plane.

4.2 Ignition Transient of the LCSCI element

The ignition process of the LCSCI element is visualized in Figure 9. By superimposing the OH* high-speed images onto the Schlieren images at defined times, the reaction zone and its expansion during the ignition transient can be visualized in unison with LOX spray features and distribution. At $t = +0.1$ ms (a) the first laser pulse is generated and creates a ignition plasma at the shear layer between the propellants close to the injector exit. From here the flame kernel expands in the mixing zone, but still staying on the topside of the spray, where the laser pulse was placed (b-c). Only after roughly 1.0 ms does the reaction zone expand around the whole circumference of the injector and into the recircularization zone (d-e). During this time, pressure and temperature rise inside the combustion volume evaporates the small LOX droplets and forces residual LOX out of the nozzle as well, resulting in the clearing up of the window (e-f). Subsequently, said pressure rise forces combustion chamber gases back into the injector post, leading to a temporary cut-off of fresh LOX supply and resulting in a breakdown of the gaseous core and annular liquid film. This can be seen in Figure 9(f-i), where no distinct LOX core can be identified and spray and flame expansion angles are diminished. This effect can also be seen in pressure traces in Figure 5, where the LOX side pressure drop becomes negative for a short amount of time after ignition. This LOX swirl breakdown can be seen until 8.9 ms, when the effects of the initial pressure peak ease up. At roughly 100 ms a quasi steady-state operation is reached. Figure 9(j) depicts the onset of this phase, with high-intensity reaction zones able to be identified close to the injector around the visible LOX core as well as further downstream. Lower intensity emissions are also present in the entirety of the recircularization zone beside the injector nut, leading to potentially high faceplate heat loads in this area. Summarized, the ignition behavior of the element is considered good, with no signs of a significant flame liftoff during or after the ignition process. Even during

the temporary breakdown of the LOX swirl inside the post, the flame seems to be anchored at the injector element's exit.

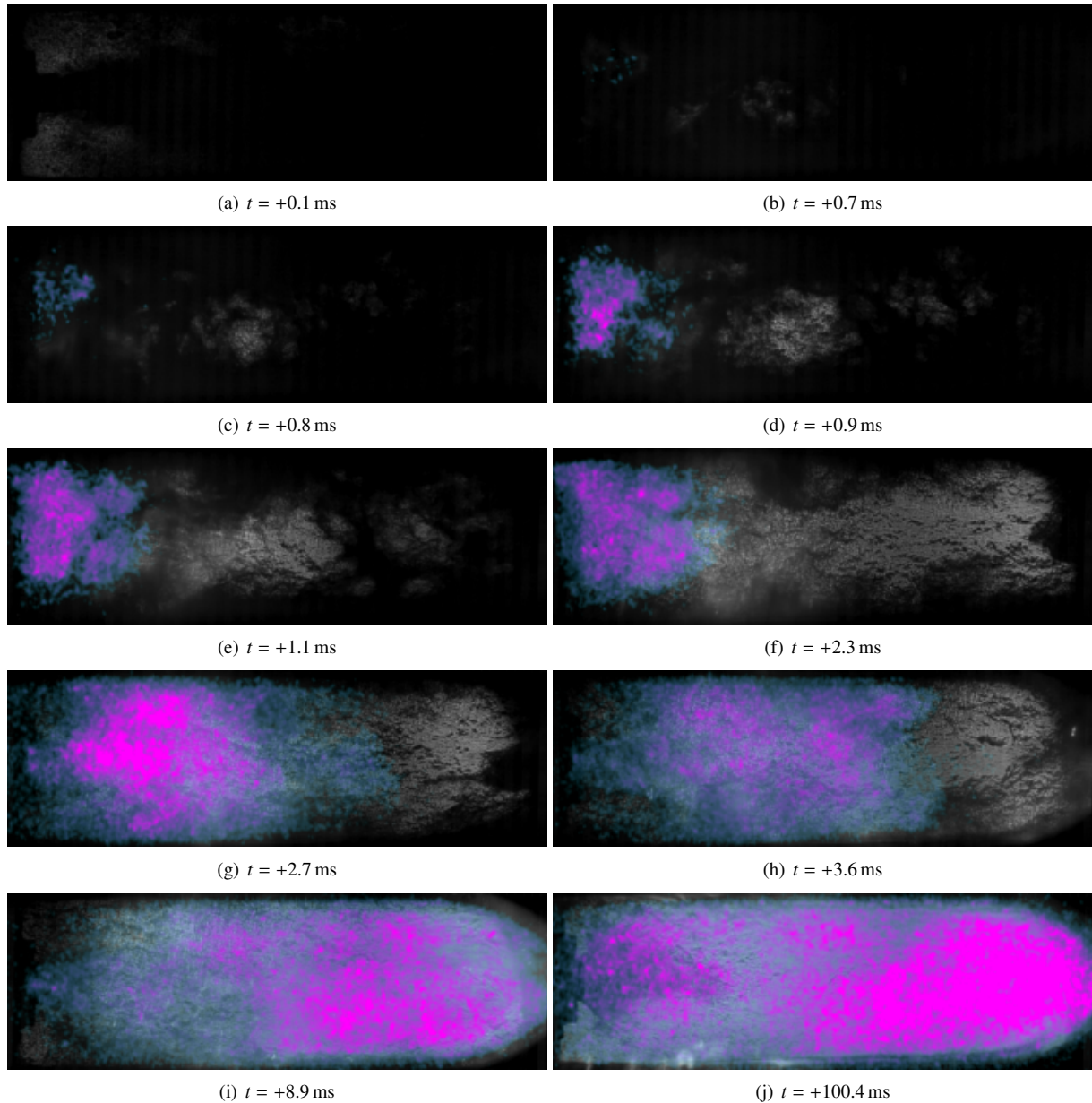


Figure 9: Superposition of instantaneous high-speed Schlieren (background) and OH* (violet/blue) images during ignition and first stages of startup transient (counter-swirling CH₄-configuration)

5. Conclusions and Outlook

Three different LOX/CH₄ LCSCI configurations were designed and hot-fired in an optically accessible research combustor at the M3.1 testbench of the German Aerospace Center (DLR) in Lampoldshausen, Germany. These configurations all featured a tangential inlet type pressure swirl LOX injector. CH₄ injection geometry was varied between the three configurations creating a classical coaxial injection as well as co- and counter-swirling element types. The experiments were accompanied by an optical diagnostics setup, consisting of a high-speed Schlieren visualization system and an image intensified high-speed camera for capturing OH*-emissions.

A pulsed laser ignition system was successfully used to ignite the swirl injector elements. The ignition process was captured with the high-speed cameras and subsequently investigated (test goal 1). During the tests chamber pressures of 2.5 – 3.2 bar were targeted, while mass flow rates ranged between 61 and 71.2 g/s for LOX and 17.9 and

20.1 g/s for CH₄. The injector element performed as expected with no signs of flame lifting during or after the ignition process. For low element mass flow rates, LF instabilities could be seen for all injector configurations. Higher flow rates and chamber pressures eliminated the instabilities (test goal 2).

The tests conducted in this study further showed that the injector element with counter-swirling CH₄ injection featured shorter LOX core lengths during hot-fire operation and potentially faster propellant mixing, resulting in higher flame intensity closer to the injector exit. Therefore, the counter-swirling configuration is determined to be the most promising of the three configurations (test goal 3). Subsequently, this element configuration is chosen for the future representative fullscale hot-fire campaign at the DLR science and technology testbench P8.

References

- [1] ABRAMOVICH, G. The theory of swirl atomizer, industrial aerodynamics. Tech. rep., Moscow: Bureau of Advanced Technology, Central Institute of Aerohydrodynamics, 1944.
- [2] AHN, J., K.AHN, AND LIM, H. Y. Injection properties according to the inner shape of metal additive layer manufactured coaxial injectors. *Journal of Applied Fluid Mechanics* 15, 4 (jul 2022).
- [3] BEE, A. Design and experimental comparison of swirl coaxial and shear coaxial injector elements for main combustion chambers of lox/lng engines (in german). Master's thesis, University of Stuttgart, 2021.
- [4] BEER, J. M., AND CHIGIER, N. A. *Combustion Aerodynamics*. Applied Science Publishers Limited, 1972.
- [5] BOERNER, M., TRAUDT, T., KLEIN, S., AND HARDI, J. Overview of the dlr m3 test field for component testing for cryogenic propulsion. In *3rd Ground-based space facilities symposium 2022. 3rd Ground-Based Space Facilities Symposium, Marseille, France (2022)*.
- [6] EURY, S., GASTAL, J., AND BORROMEE, J. Development status of the vulcain engine.
- [7] GREENE, C., WOODWARD, R., PAL, S., AND SANTORO, S. Design and study of a lox/gh2 throttleable swirl injector for rocket applications. Tech. rep., Propulsion Engineering Research Center, Department of Mechanical and Nuclear Engineering, The Pennsylvania State University, 2002.
- [8] IANNETTI, A. Prometheus, a lox/lch4 reusable rocket engine.
- [9] JOST, R. Investigation of flame anchoring and flame extinction during the ignition process of lox/gch4 (in german). Master's thesis, University of Stuttgart, 2020.
- [10] KAESS, R., KOEGLMEIER, S., BEHR, R., KNAB, O., SAUCERAU, D., DESENLIS, M., VINGERT, L., NICOLE, A., SCHMITT, T., DUCRUIX, S., THERON, M., LEQUETTE, L., VAN SCHYNDEL, J., HORCHLER, T., HARDI, J., ARMBRUSTER, W., CUENOT, B., AND BLANCHARD, S. Rest hf-10 test case: Synthesis of the contributions for the simulation of excited methane flames under real gas conditions.
- [11] KIM, S., KHIL, T., KIM, D., AND YOON, Y. Effect of geometric parameters on the liquid film thickness and air core formation in a swirl injector. *Measurement Science and Technology* 20, 1 (dec 2008), 015403.
- [12] KLEIN, S., BOERNER, M., HARDI, J., SUSLOV, D., AND OSCHWALD, M. Injector-coupled thermoacoustic instabilities in an experimental LOX-methane rocket combustor during start-up. *CEAS Space Journal* 12, 2 (jan 2020), 267–279.
- [13] LECHTENBERG, A., AND GERLINGER, P. Rest hf-10 test case: Flame response to forced excitation of a methane driven rocket combustion chamber.
- [14] MARTIN, J., ARMBRUSTER, W., STUETZER, R., GENERAL, S., KNAPP, B., SUSLOV, D., AND HARDI, J. Flame characteristics of a high-pressure lox/h2 rocket combustor with large optical access. *Case Studies in Thermal Engineering* 28 (dec 2021), 101546.
- [15] MARTIN, J., BOERRNER, M., HARDI, J., SUSLOV, D., AND OSCHWALD, M. Experimental investigation of flame anchoring behavior in a LOX/LNG rocket combustor. *Aerospace* 10, 6 (jun 2023), 542.
- [16] SALGUES, D., MOUIS, A.-G., LEE, S.-Y., KALITAN, D., PAL, S., AND SANTORO, R. Shear and swirl coaxial injector studies of LOX/GCH4 rocket combustion using non-intrusive laser diagnostics.
- [17] YANG, L.-J., GE, M.-H., ZHANG, M.-Z., FU, Q.-F., AND CAI, G.-B. Spray characteristics of recessed gas-liquid coaxial swirl injector. *Journal of Propulsion and Power* 24, 6 (nov 2008), 1332–1339.